J Physiol 589.10 (2011) pp 2543–2558

The Journal of Physiology

Population calcium imaging of spontaneous respiratory and novel motor activity in the facial nucleus and ventral brainstem in newborn mice

Karin Persson and Jens C. Rekling

Department of Neuroscience and Pharmacology, Copenhagen University – Panum Institute – 12.3, Blegdamsvej 3, DK-2200 Copenhagen N, Denmark

Non-technical summary The brainstem contains neural circuits that control breathing. Groups of neurons produce the rhythm of inspiration and expiration, and other groups produce the motor output that controls respiratory muscles. One such group of neurons is the facial nucleus, which controls muscles in the face. Here we show, using electrical and calcium imaging techniques, that different subregions within the facial nucleus are particularly active during breathing, which suggest an involvement in keeping the airway open during inspiration. Furthermore, the experiments show that a novel rhythm generating circuit is present in the brainstem. These results may help us to a better understanding of how the brainstem controls breathing and other motor behaviours in the upper body.

Abstract The brainstem contains rhythm and pattern forming circuits, which drive cranial and spinal motor pools to produce respiratory and other motor patterns. Here we used calcium imaging combined with nerve recordings in newborn mice to reveal spontaneous population activity in the ventral brainstem and in the facial nucleus. In Fluo-8 AM loaded brainstem–spinal cord preparations, respiratory activity on cervical nerves was synchronized with calcium signals at the ventrolateral brainstem surface. Individual ventrolateral neurons at the level of the parafacial respiratory group showed perfect or partial synchrony with respiratory nerve bursts. In brainstem–spinal cord preparations, cut at the level of the mid-facial nucleus, calcium signals were recorded in the dorsal, lateral and medial facial subnuclei during respiratory activity. Strong activity initiated in the dorsal subnucleus, followed by activity in lateral and medial subnuclei. Whole-cell recordings from facial motoneurons showed weak respiratory drives, and electrical field potential recordings confirmed respiratory drive to particularly the dorsal and lateral subnuclei. Putative facial premotoneurons showed respiratory-related calcium signals, and were predominantly located dorsomedial to the facial nucleus. A novel motor activity on facial, cervical and thoracic nerves was synchronized with calcium signals at the ventromedial brainstem extending from the level of the facial nucleus to the medulla–spinal cord border. Cervical dorsal root stimulation induced similar ventromedial activity. The medial facial subnucleus showed calcium signals synchronized with this novel motor activity on cervical nerves, and cervical dorsal root stimulation induced similar medial facial subnucleus activity. In conclusion, the dorsal and lateral facial subnuclei are strongly respiratory-modulated, and the brainstem contains a novel pattern forming circuit that drives the medial facial subnucleus and cervical motor pools.

(Resubmitted 10 February 2011; accepted after revision 23 March 2011; first published online 28 March 2011)
Corresponding author J. C. Rekling: Cellular and Systems Neurobiology Laboratory, Department of Neuroscience and Pharmacology, Copenhagen University – Panum Institute – 12.3, Blegdamsvej 3, DK-2200 Copenhagen N, Denmark. Email: jrekling@sund.ku.dk

Abbreviations pFRG, parafacial respiratory group; VL, ventrolateral; L,R-VL, left and right ventrolateral region; VM, ventromedial; L,R-VM, left and right ventromedial region.

DOI: 10.1113/jphysiol.2011.207225

Introduction

The brainstem contains neural circuits controlling several motor functions related to breathing (Feldman & Del Negro, 2006; Rybak *et al.* 2007). Many ingestive and facial motor behaviours are also initiated and produced by brainstem circuits (Lang, 2009). Output from these circuits is transmitted to spinal and cranial motor pools to create precise motor patterns. However, the role of premotoneurons and different motor subnuclei in transmitting and shaping motor commands from central circuits is only beginning to be unravelled. The facial nucleus, which innervates facial and auricular musculature, is involved in many orofacial and auricular behaviours. It is also an integral part of the motor programme that maintains upper airway patency during breathing (Strohl, 1985), and mastication and swallowing also involve facial motoneurons (Fay & Norgren, 1997). The nucleus receives inspiratory respiratory drive originating in the preBötzinger complex and pre/postinspiratory drive from the parafacial respiratory group (pFRG) (Onimaru *et al.* 2006; Thoby-Brisson *et al.* 2009; Bouvier *et al.* 2010). However, little is known about how these respiratory drives reach the facial nucleus, and to what extent different facial subnuclei are activated during breathing. Here we used electrical nerve recordings, whole-cell patch clamp, and calcium imaging to reveal spontaneous spatiotemporal activity patterns in the upper brainstem of P0.5–P3.5 mice in two types of *in vitro* preparations, focusing on the facial nucleus. We show that respiratory-modulated putative facial premotoneurons are located dorsomedial to the facial nucleus, and that the dorsal and lateral facial subnuclei show particularly strong respiratory activity. In addition we observed a novel bilateral activity pattern in the ventromedial brainstem, which included strong activity in the medial facial subnucleus, and motor output on facial and cervical nerves. This novel activity may represent yet another motor behaviour controlled by ventrally located brainstem circuits.

Methods

Ethical approval

All experiments and procedures were approved by the Department of Experimental Medicine, and according to procedures laid out by Danish Ministry of Justice and the Danish National Committee for Ethics in Animal Research, and conform to the principles of UK regulation, as described in Drummond (2009).

In vitro preparations, Fluo-8 AM loading and choline acetyltransferase immunolabelling

Neonate (day 0.5–3.5) US Naval Medical Research Institute (NMRI) mice were anaesthetized with isoflurane, and killed with a cut across the thorax and removal of the heart and lungs. The neuraxis was removed by dissection in an ice cold, oxygenated (95% O_2–5% CO_2) solution containing (in mM): 250 glycerol (Ye *et al.* 2006), 3 KCl, 5 KH_2PO_4, 36 $NaHCO_3$, 10 D-(+)-glucose, 2 $MgSO_4$ and 0.7 $CaCl_2$. Two preparations were made. The first was the brainstem–spinal cord preparation, which contained the entire brainstem, including the pons, and the cervical and sometimes upper thoracic part of the spinal cord. Large vessels and the pia mater were removed from the ventral surface. The second was the mid-facial brainstem–spinal cord preparation, where the brainstem–spinal cord was glued (using cyanoacrylate) to a piece of filter paper, and mounted upright on an agar block at a ventro-dorsal tilt of 25 deg. Large vessels were removed, but the pia mater was left intact. A cut was placed at the level of the mid-facial nucleus, which was reached by cutting two 150 μm sections starting at the most rostral border of the facial nucleus, which was readily visible in the dissecting microscope, using a vibrating-blade microtome (Microm HM 650 V, Walldorf, Germany). Both types of preparations were loaded with the Ca^{2+}-sensitive dye Fluo-8 AM (AAT Bioquest, Sunnyvale, CA, USA) by placing the preparations in a loading solution for 1–1.5 h at room temperature under bubbling with 95% O_2–5% CO_2. The loading solution was prepared by dissolving 50 μg Fluo-8 AM in 50 μl dimethyl sulfoxide (DMSO), combining 20 μl of this solution with 5 μl Cremophor EL (Fluka, St Louis, MO, USA) and 5 μl 20% Pluronic F-127 in DMSO (AAT Bioquest), adding these 30 μl to 1 ml artificial cerebrospinal fluid (ACSF) with 100 mM D-mannitol (improving dye diffusion into the tissue (Funke *et al.* 2007; Sigma-Aldrich, St Louis, MO, USA), and 100 μM MK-571 (a multidrug resistance transport blocker improving calcium indicator dye uptake (Manzini *et al.* 2008; Sigma-Aldrich). The final Fluo-8 AM concentration was 20 μM. Following loading with Fluo-8 AM, the dorsal surface of both preparations was glued to a piece of filter paper, the dorsal surface of mid-facial brainstem–spinal cord preparation was further glued to a triangular silver block, and the preparations were transferred to a recording chamber, mounted with the ventral or rostral surface up.

In some brainstem–spinal cord preparations, where a sagittal vibrating-blade microtome cut was placed along the facial nucleus, calcium imaging was followed by overnight fixation (4% paraformaldehyde in 0.1 M Sorensen phosphate buffer). Unsectioned preparations

were then incubated under constant agitation in diluted choline acetyltransferase (ChAT) antibody solution (anti-ChAT, cat no. AB143, Millipore, Billerica, MA, USA; dilution 1:100, 18 h, room temperature). To reveal ChAT immunoreactivity, preparations were treated with swine anti-rabbit immunoglobulin–biotin (dilution 1:300, 12 h, 4°C; DAKO, Glostrup, Denmark), followed by a peroxidase reaction using the Vectastain ABC kit (peroxidase standard PK4000, Vector Laboratories, Burlingame, CA, USA). The resulting dark reaction product, which was located at the surface of the preparation at the level of the facial nucleus, was observed and photographed on the same stereomicroscope that was used for calcium imaging.

Nerve, field potential and whole cell recordings

Nerve and optical recordings commenced 30 min after the preparation was placed in the recording chamber, and stabilized by placing a silver frame on the filter paper. The recording chamber had a volume of 2 ml and temperature of 29.0°C and was constantly superfused at a rate of 2 ml min^{-1} with preheated oxygenated (95% O_2–5% CO_2) ACSF. The ACSF contained (in mM): 130 NaCl, 5.4 KCl, 0.8 KH_2PO_4, 26 $NaHCO_3$, 30 D-(+)-glucose, 1 $MgCl_2$ and 0.8 $CaCl_2$. The surface of the preparation was illuminated by high-luminosity LEDs (HLV series, CCS LED Spotlight, Kyoto, Japan) and visualized by a fluorescence stereo microscope (Leica MZ16 FA, Wetzlar, Germany). Glass-pipette suction electrodes (tip diameter of 40–160 μm, A-M Systems, Carlsborg, WA, USA) were placed on VII, cervical, or thoracic rootlets to record spontaneous nerve activity. The relative anatomical location of the facial nucleus was determined by thionine (1% in 0.1 M sodium acetate trihydrate–0.1 M acetic acid) labelling of consecutive 100 μm thick sections from reference preparations. Field potential recording from the facial nucleus was performed using the same pipette type as used for whole-cell patch clamp, but filled with ACSF. The outside of the pipette tip was labelled with red ink obtained from permanent pens (Staedtler). This made it possible to place the pipette in eight positions (estimated depth 50–100 μm) within the facial nucleus under visual control, and an image was taken at each position for offline reconstruction. Nerve and field potentials were amplified by a custom built nerve amplifier (×50,000), filtered at DC–2 kHz, and digitized (2.5 kHz) by a PCI-6289, M Series A/D-board (National Instruments, Austin, TX, USA) controlled by Igor Pro (Wavemetrics, Lake Oswego, OR, USA) software. For whole cell recordings neurons located in the facial nucleus were visualized using an Olympus BX51 (upright, modified to be fixed stage, mounted on an XY platform) with an ×2.5 and an ×63 objective. The ×2.5 objective was used to visualize the entire cut surface of the preparation. The ×63 objective was used in conjunction with oblique illumination optics to visualize the soma of individual neurons and the recording pipette tip. The preparation was illuminated from below using a 100 W halogen lamp, and the image was acquired by a EMCCD camera (Andor LucaEM S DL-658M, 658 × 496 pixels, Andor Technology, Belfast, UK), software contrast enhanced (SOLARIS, Andor Technology), and displayed on a PC monitor. Glass micropipettes were pulled from filamented glass tubes (outer diameter 1.5 mm, inner diameter 0.86 mm, Harvard Apparatus, Holliston, MA, USA) using a PUL-100 micropipette puller (World Precision Instruments, Sarasota, FL, USA) and filled with a solution containing (in mM): 145 potassium D-gluconate, 10 NaCl, 1 $MgCl_2$, 0.01 $CaCl_2$, 0.1 BAPTA (1,2-bis(2-aminophenoxy)ethane-*N*,*N*,*N*′*N*′-tetraacetic acid, tetra-K^+ salt), 10 Hepes, 3 ATP (Mg^{2+}), 0.3 GTP (Na^+), pH 7.3. Recording pipettes were mounted in a HS-2 headstage (gain 0.01) and current clamp recordings performed with an Axoclamp 2B amplifier (Molecular Devices, Sunnyvale, CA, USA). Pipette resistance before seal formation was typically 2–3 MΩ and after the whole cell configuration was achieved series resistance was 5–20 MΩ. All recordings were corrected for a liquid junction potential of 14 mV (calculated using Clampex software, Molecular Devices). Input resistance was measured by applying a small amplitude (0.05–0.1 nA, 500 ms) hyperpolarizing current pulse from resting membrane potential giving rise to a membrane deflection of no more than 10 mV. Resting membrane potential was measured as an unbiased membrane potential recording minus the extracellular potential measured after the recording electrode was pulled out of the cell. Criteria for suitable whole-cell recording were stable input resistance for more than 10 min.

Antidromic and dorsal root stimulation

Antidromic stimulation of facial motoneurons was done using a concentric bipolar stimulus electrode (Outer Pole: 125 μm, Inner Pole: 25 μm, FHC Inc., Bowdoin, ME, USA) placed in the dorsomedial area of the cut rostral surface (approximate position of the genu of the facial nerve). A train of 10 pulses (2 ms duration, 50 ms interval) was delivered every 2–4 s by a monophasic stimulus isolator (IsoFlex, A.M.P.I., Jerusalem, Israel) at current strengths 10–400 μA. The correct position of the stimulation electrode was confirmed by visualization of successful antidromic invasion of the facial nucleus by live imaging with online subtraction of a background image taken prior to stimulation. Stimulation of dorsal nerve rootlets was done using the same glass-pipette suction electrodes as used for the nerve recordings. The suction electrode was placed on the dorsal root (DR-C2, DR-C4–8,

DR-T2–3) and connected to the monophasic stimulus isolator. Stimulation was given every 4 s, by a train of 10 pulses with duration 500 μs at 50 ms interval, at current strengths of 0.02–5 mA.

Optical recordings

For detection of Fluo-8 fluorescence, a metal halide light source (Leica EL6000, Wetzlar, Germany) was coupled to the stereo microscope via a liquid light guide, and appropriate optical filters (Leica GFP3: excitation 470/40 nm; barrier 525/50) were used. Live image stacks were captured by an EMCCD camera (Andor LucaEM S DL-658M, Andor Technology), controlled by SOLIS software (Andor Technology). Imaging was done using magnification of ×40–115, at sampling rates of 3–70 frames s^{-1} (3 frames s^{-1} unbinned, 70 frames s^{-1} 2×2 binning), in image sessions lasting 6–150 s. Substantial bleaching of the Fluo-8 fluorescence was noted throughout the longer imaging session, which was partially corrected for during the analysis using a running background subtraction (1 s back in time).

Analysis and statistics

Analysis of nerve, field potentials, patch clamp and optical recordings was done offline using Igor Pro (Wavemetrics), Clampex (Molecular Devices), and ImageJ (National Institutes of Health, Bethesda, MD, USA, http://rsbweb.nih.gov/ij/). Raw image stacks were partially corrected for bleaching of the Fluo-8 dye, and turned into image stacks showing relative changes in fluorescence (ΔF) by subtracting the image 1 s before each frame in the stack. To construct a cycle-triggered-averaged (CTA) image of the ΔF stack, a custom program was made in Igor Pro executing the following procedure: (1) ΔF image stacks were Kalman filtered, and colour coded (rainbow, RGB, black: small ΔF; red to white: large ΔF), (2) the raw nerve signal was used to detect the onset time of inspiratory activity, (3) an image was pulled out from the image stack corresponding to the peak of inspiratory activity, and an image 1 s prior was subtracted from this image, (4) an averaged image was constructed by averaging 5–40 of these baseline-subtracted inspiratory-related images. Finally, the averaged image was 2- to 10-point mean-filtered (mean of adjacent 2×2 to 10×10 points), and brightness and contrast enhanced using ImageJ. In some experiments regions of interest (ROIs) were defined and average ΔF values within the ROI were plotted *versus* time or used for CTA plots showing ΔF and nerve signals. Relative onset times were determined by baseline departures in differentiated traces of the ΔF and nerve signal. The duration of the calcium signal was calculated as the difference between times of the rising and falling phases at the half-amplitude points. It should be noted that the recorded amplitude of nerve signals is strongly dependent on resistance between the glass-pipette suction electrodes and the nerve, and the fluorescence output from Fluo-8 AM labelled tissue is dependent on loading time, age of the animal, light exposure time, and quenching – all variables that changed substantially from experiment to experiment. For these reasons amplitude calibration bars on nerve traces and ΔF images have little meaning, and have been omitted from the figures. However, the relative changes in the data within one experiment has meaning, and can be distinguished as relative changes in nerve signal amplitude or colour code in single traces or images. Contrast and display range were kept constant when showing several images from the same experiment. Statistical values are given as means ± SD, and Student's *t* test was used for statistical comparisons.

Results

To reveal spontaneous spatiotemporal activity patterns in the upper brainstem of P0.5–P3.5 mice, electrical nerve recordings and calcium imaging were combined in two types of preparations. In the first, nerve recordings and imaging of the ventral brainstem surface were combined using a preparation containing the brainstem and upper spinal cord. In the second, a transverse cut was placed through the brainstem at the level of the facial nucleus, retaining caudal structures down to the cervical spinal cord, and nerve recordings were combined with imaging of the cut rostral surface. The optimized Fluo-8 AM loading protocol allowed for visualization of large-scale population activity, subnuclei activity, and single cell activity.

Respiratory and novel motor activity in cervical nerves and ventral brainstem

Previously described respiratory burst activity on VII, and cervical nerves (Onimaru *et al.* 2006) was observed in the brainstem–spinal cord preparation (5.2 ± 2.7 burst min^{-1}), synchronized with calcium signals from the ventrolateral respiratory column (Fig. 1 and supplementary movie 1, $n = 27$ brainstem–spinal cord preparations). However, a novel non-respiratory motor pattern was also observed in 15 of 49 preparations (N – Fig. 1*B*, $n = 13$ brainstem–spinal cord, $n = 2$ mid-facial brainstem–spinal cord). In the nerve recordings this novel motor activity occurred in the same nerves as respiratory activity ($n = 43$ nerves; facial $n = 2$, C1–C2 $n = 2$, C3–C5 $n = 22$, C6–C8 $n = 14$, T1–T3 $n = 2$, T8 $n = 1$) and in several cranial and spinal nerves recorded simultaneously (Fig. 1*B*). The novel motor activity on nerves was faster (10.2 ± 5.4 burst min^{-1}, $P < 0.001$),

more variable (inter-burst interval coefficient of variation: $110 \pm 57\%$, $P < 0.001$, $n = 13$), than respiratory activity (inter-burst interval coefficient of variation: $25 \pm 9\%$, $n = 26$). The novel motor activity appeared as individual or double bursts ($n = 6$), or trains or clusters of bursts ($n = 7$), with identical patterns in different co-recorded nerves, and had variable amplitude between preparations relative to the amplitude of the respiratory activity (not shown).

A CTA image of the ΔF from the Fluo-8 AM labelled brainstem surface triggered off respiratory nerve activity showed ventrolateral (VL) population activity bilaterally, shaped as a hook, and located along the lateral border of the facial nucleus, extending caudally along the ventral surface (Fig. 1*C*). The active region was 200 μm wide, 569 μm long (core region), and 1067 μm in total length. Group data showed a width of 230 ± 42 μm ($n = 13$), core length of 600 ± 67 μm ($n = 13$) and total length of 1092 ± 56 μm ($n = 6$, some population activity extended beyond the image plane). The region corresponds to the pFRG and ventral respiratory column as previously described (Onimaru & Homma, 2003). Calcium signals from ROIs encircling the left and right ventrolateral region (L,R-VL) were bilaterally synchronized, and in phase with each respiratory nerve burst (Fig. 1*B* and *F*). Surprisingly, the novel motor activity on VII and cervical nerves was synchronized with population activity in a novel ventromedial region at the brainstem surface (Fig. 1*B* and *D*).

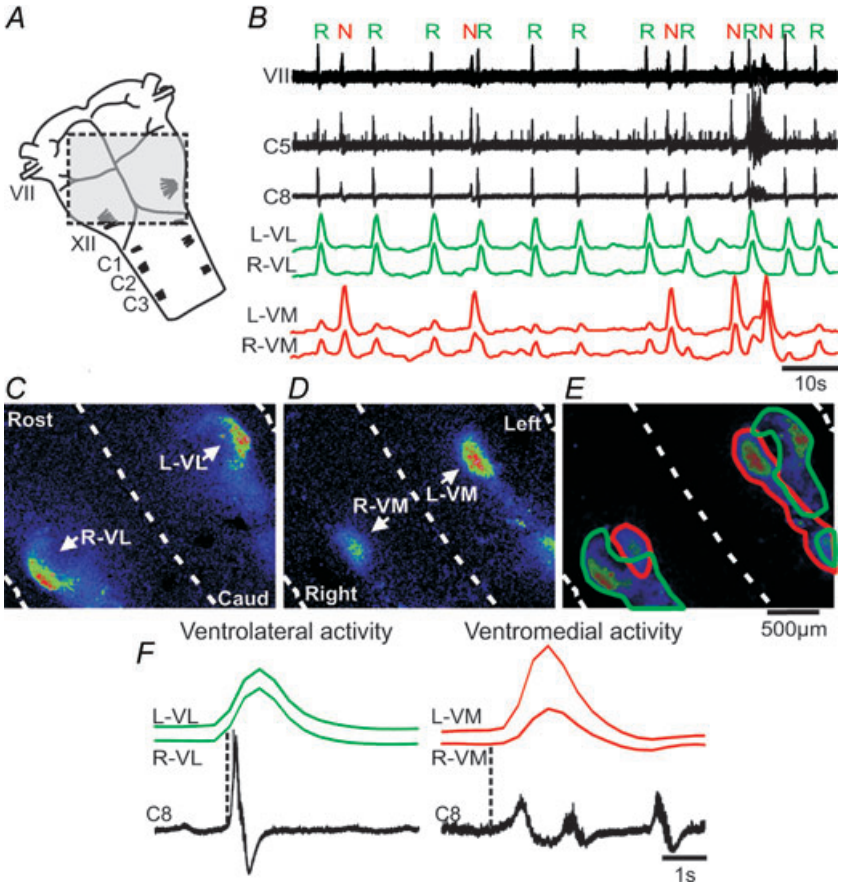

Figure 1. Two different motor patterns on facial and cervical nerve rootlets are synchronized with population activity in the ventrolateral and ventromedial brainstem
A, brainstem–spinal cord preparation illustrating the field-of-view used to image population activity over the ventral surface (shaded area); VII, facial nerve; XII, hypoglossal rootlets; C1, first cervical nerve. *B*, spontaneous nerve activity recorded from facial (VII) and cervical (C5 and C8) rootlets (left side), and traces showing the ΔF over left, right ventrolateral surface (L,R-VL, green traces), and left, right ventromedial surface (L,R-VM, red traces). Note the regular respiratory activity (R), and irregular novel motor activity (N) in the nerve recordings. *C*, CTA image triggered off the respiratory nerve activity (16 cycles) showing bilateral population activity along the ventrolateral surface. Rost, rostral; Caud, caudal. Dashed lines demark midline and lateral boundaries of the preparation. *D*, CTA image triggered off the novel motor nerve activity (7 cycles) showing bilateral population activity along the ventromedial surface. *E*, overlay of the CTA images from the respiratory and novel motor activity outlining ventrolateral (green), and ventromedial (red) population activities. *F*, left panel, averages of respiratory nerve activity and ΔF traces from L- and R-VL (16 cycles), Right panel, averages of novel motor nerve activity and ΔF traces from L- and R-VM (7 cycles). Dotted lines indicate onset of nerve activity.

A CTA image triggered off the novel motor nerve activity showed ventromedial (VM) activity bilaterally, and shaped as an elongated column extending caudally from the level of the medial part of the facial nucleus (Fig. 1*D*). The active region was 254 μm wide, 468 μm long (core length) and 1510 μm in total length. Group data showed a width of 234 ± 29 μm ($n = 10$), length of 445 ± 52 μm ($n = 10$) and total length of 1391 ± 191 μm ($n = 4$, age P0.5–P1.5, some population activity extended beyond the image plane). Calcium signals from ROIs encircling the left and right ventromedial region (L,R-VM) were bilaterally synchronized, and in phase with each novel motor activity burst (Fig. 1*B* and *F*). Overlay of the CTA images from the ventral surface confirmed the location of the novel ventromedial region being medial to the pFRG on both sides with some overlap with the caudal part of the respiratory column (Fig. 1*E*). Group data (cervical nerves combined) of the averages of respiratory nerve activity and ΔF traces from L- and R-VL showed a nerve burst duration of 1.3 ± 0.4 s, start of the calcium signal relative to the start of the nerve burst of −303 ± 286 ms (i.e. before), and calcium signal duration of 1.1 ± 0.1 s (Fig. 1*F*, left panel, $n = 27$). Group data of the averages of the novel motor nerve activity and ΔF traces from L- and R-VM showed a nerve burst duration of 2.1 ± 0.6 s ($P < 0.0001$ compared to the nerve burst duration of the respiratory calcium signal), start of the calcium signal relative to the start of nerve burst of 193 ± 120 ms (i.e. after, $P < 0.0001$ compared to the relative start of the respiratory calcium signal), and calcium signal duration of 1.3 ± 0.2 s (Fig. 1*F*, right panel, $n = 11$).

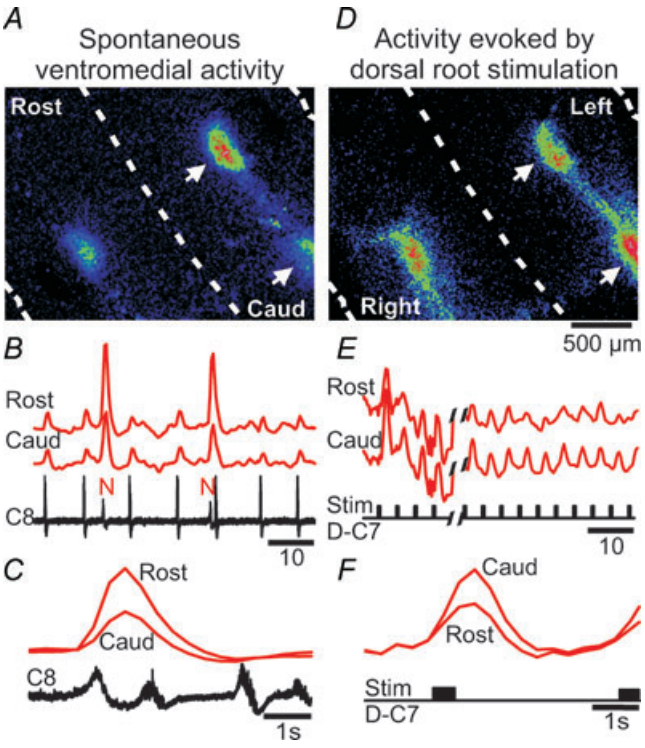

Figure 2. Electrical stimulation of a cervical dorsal root induces population activity at the ventromedial region
A, CTA image triggered off spontaneous novel motor nerve activity (7 cycles) showing bilateral population activity along the ventromedial surface, in particular in rostral and caudal regions. *B*, spontaneous nerve activity recorded from cervical (C8) rootlet, and traces showing the ΔF over rostral, and caudal regions at the ventromedial surface (red traces). N: novel motor nerve activity. *C*, averages of novel motor nerve activity (7 cycles) and ΔF traces from rostral and caudal regions (red traces, corresponding to arrows in *A*). Note that rostral and caudal regions are synchronized. *D*, CTA image triggered off left cervical dorsal stimulations (D–C7, 7 stimuli), showing bilateral population activity along the ventromedial surface. Note that the stimulus evoked activity is bilateral, and located in the same ventromedial regions as the spontaneous activity in *A*. *E*, dorsal root stimulus-evoked ΔF over rostral, and caudal regions at the ventromedial surface (red traces). *F*, averages of dorsal root stimulus-evoked ΔF (7 cycles) from rostral and caudal regions (red traces, corresponding to arrows in *D*).

Dorsal root stimulation induce population activity at the ventromedial brainstem surface

Calcium imaging of the spontaneous ventromedial population activity showed a characteristic pattern with strong ΔF at the rostral and caudal pole of the elongated column of activity (Fig. 2*A*). Calcium signals from ROIs encircling these rostral and caudal ventromedial regions (Fig. 2*A*, arrows) were synchronized, and in phase with each novel motor nerve burst (Fig. 2*B* and *C*). The rostral region showed relatively larger ΔF than the caudal region (Fig. 2*A* and *C*, $P < 0.05$, $n = 4$ brainstem–spinal cord preparations). Interestingly, the same ventromedial activity pattern (duration: 1.1 ± 0.1 s) could be evoked by electrical stimulation of cervical (C7) dorsal root using trains of stimuli (500 ms epochs: 10 times 500 μs stimuli with 50 ms interval, given every 4 s, Fig. 2*D*–*F*). Stimulation of the cervical dorsal root at one side (left) induced ventromedial activity at both sides (Fig. 2*D*). Bilateral ventromedial activity could be evoked by stimulation of several different dorsal roots (C2, C4–C8, T2, $n = 7$ brainstem–spinal cord preparations). Each train of stimulation triggered ventromedial activity (Fig. 2*E*). However, the stimulus-locked ΔF decreased rapidly during the first four trains, and stabilized after three to five stimulus trains ($n = 6$, Fig. 2*E*). Calcium signals from ROIs encircling rostral and caudal ventromedial regions (Fig. 2*A*, arrows) were synchronized, and in phase with each electrical stimulus (Fig. 2*E*).

Visualization of single cells in ventrolateral and ventromedial regions

The somas of individual cells were visible along the surface in both ventrolateral and ventromedial regions at higher optical magnifications (Fig. 3). ROIs around the overall

ventrolateral region (Fig. 3*A*,VL), and some individual cells (Fig. 3*A*, cells 1–4) showed activity synchronized with the respiratory C4 nerve activity ($n = 21$ brainstem–spinal cord preparations). The VL-ROI was active at every respiratory burst, whereas individual cells were active at some, but not all, respiratory bursts (Fig. 3*A*, green traces). Large peaks in the cellular ROI trace correspond to the cell being active, whereas small peaks are likely to be due to the population background influencing the signal. A CTA image triggered off the C4 respiratory nerve bursts showed activity in the ventrolateral region, and individual cells appeared to be located close to the ventral surface since their somas were readily visible (cells 1–4, Fig. 3*B*). Dendrites could be partly seen around several cells within the ventrolateral region. One dendrite extending from a cell (Fig. 3*B*, asterisk) could be followed for some distance (Fig. 3*C*). Averages triggered off the C4 respiratory nerve bursts showed synchronized calcium activity in the soma and proximal and distal dendrites (Fig. 3*D*). Initiation of the calcium signal in the soma and proximal dendrite occurred at ~0.9 s before the nerve burst, whereas the distal dendrite appeared to initiate later (~0.2 s before the nerve burst), but the low signal/noise ratio makes it impossible to determine if this difference is real or an artefact reflecting inadequate sensitivity or the inability to detect the onset of dendritic changes. The somas of individual cells were also visible at the surface of the brainstem in the ventromedial region ($n = 8$ brainstem–spinal cord preparations), and two cells in this experiment showed strong calcium signals phase-locked to the novel motor nerve activity on the C5 nerve (Fig. 3*E* and *F*).

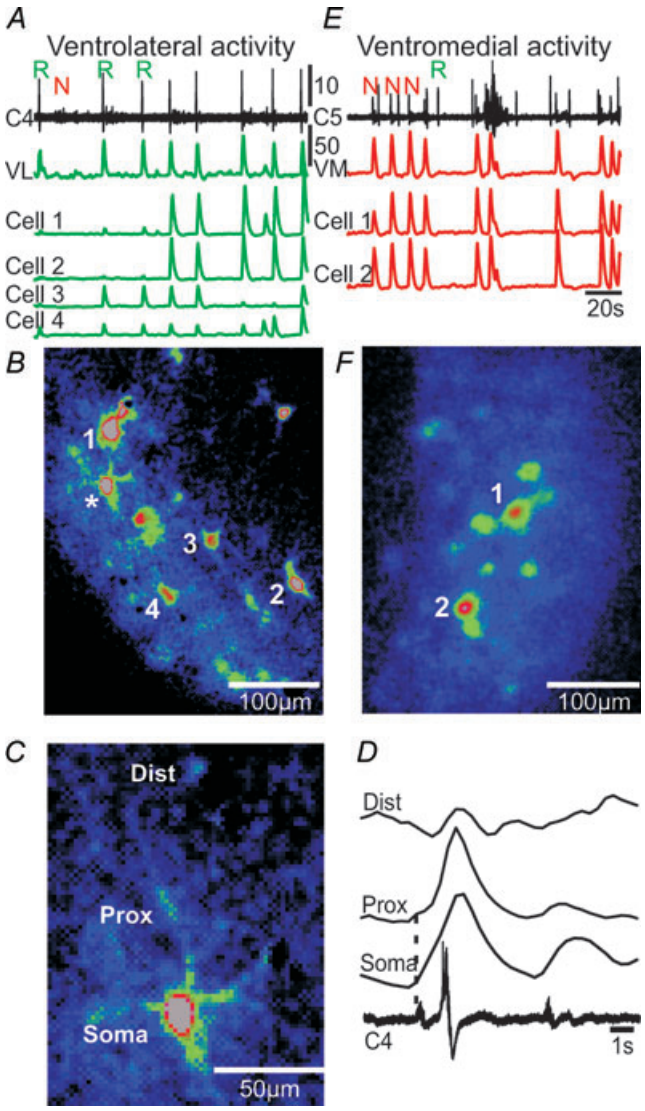

Figure 3. Calcium signals from single neurons at the ventrolateral and ventromedial surface
A, spontaneous respiratory (R) and novel motor (N) nerve activity recorded from cervical (C4) rootlet, and traces showing the ΔF over the ventrolateral surface (VL, green trace), and single neurons (cells 1–4, green traces) at the ventrolateral surface. *B*, CTA image from the ventrolateral surface triggered off cervical nerve (C4, 8 cycles) showing the location of cells 1–4, and a respiratory-modulated cell (∗), which is shown in higher magnification in *C*. *C*, single ventrolateral neuron showing dendritic loading of Fluo-8 AM. *D*, average of ΔF (8 cycles) over the soma, proximal dendrite (Prox) and distal dendrite (Dist), and respiratory activity on the cervical (C4) root. Dotted line indicates onset of somatic ΔF. Note that a calcium signal is present in the proximal and distal dendrite of the neuron. *E*, spontaneous respiratory (R) and novel motor (N) nerve activity recorded from cervical (C5) rootlet, and traces showing the ΔF over the ventromedial surface (VM), and single neurons (cells 1 and 2, red traces) at the ventromedial surface. *F*, CTA image from the ventromedial surface triggered off cervical nerve (C5, 9 cycles) showing the location of cells 1 and 2.

Respiratory and novel motor activity in facial subnuclei

Calcium imaging of the cut rostral surface of mid-facial brainstem–spinal cord preparations was performed to reveal activity patterns in different facial subnuclei (Fig. 4). Respiratory activity on cervical nerves in mid-facial brainstem–spinal cord preparations had a burst duration of 1.0 ± 0.4 s and a frequency of 8.3 ± 2.5 burst min^{-1} ($n = 22$), which was faster than in the brainstem–spinal cord preparations ($P < 0.001$). Novel motor activity on cervical nerves was only recorded in 2 of 22 mid-facial brainstem–spinal cord preparations, and had a burst duration of 3.5 ± 0.5 s and a frequency of 2.9 ± 0.2 burst min^{-1}. The boundary of the facial nucleus in the transverse plane was identified in two ways. Firstly, average Z-stack projections of the raw Fluo-8 AM images produced an image where the approximate boundary of the facial nucleus was visible due to the dense packing

of facial motoneurons (Fig. 4*A*). Secondly, antidromic activation of facial motoneurons was performed by placing a bipolar stimulating electrode in the internal facial genu at the dorsomedial part of the cut transverse surface (Fig. 4*B*, $n = 7$ of 22 mid-facial brainstem–spinal cord preparations). Antidromic stimulation induced a strong ΔF signal over the entire facial nucleus (Fig. 4*C*), starting ~30 ms after the stimulus (Fig. 4*B*, lower trace). A CTA image of the facial nucleus triggered off respiratory activity on an ipsilateral cervical nerve (C5, Fig. 4*D*) showed a strong ΔF in the dorsal facial subnucleus (Fig. 4*E* and *F*, $n = 18$ mid-facial brainstem–spinal cord preparations), and a weaker signal in the lateral (Fig. 4*E*, $n = 17$) and medial (Fig. 4*E*, $n = 5$) subnuclei. In the two experiments, that showed novel motor activity on cervical nerves, both experiments showed a strong ΔF signal only in the medial facial subnucleus in synchrony with the nerve activity (Fig. 4*G* and *H*). Optical burst activity

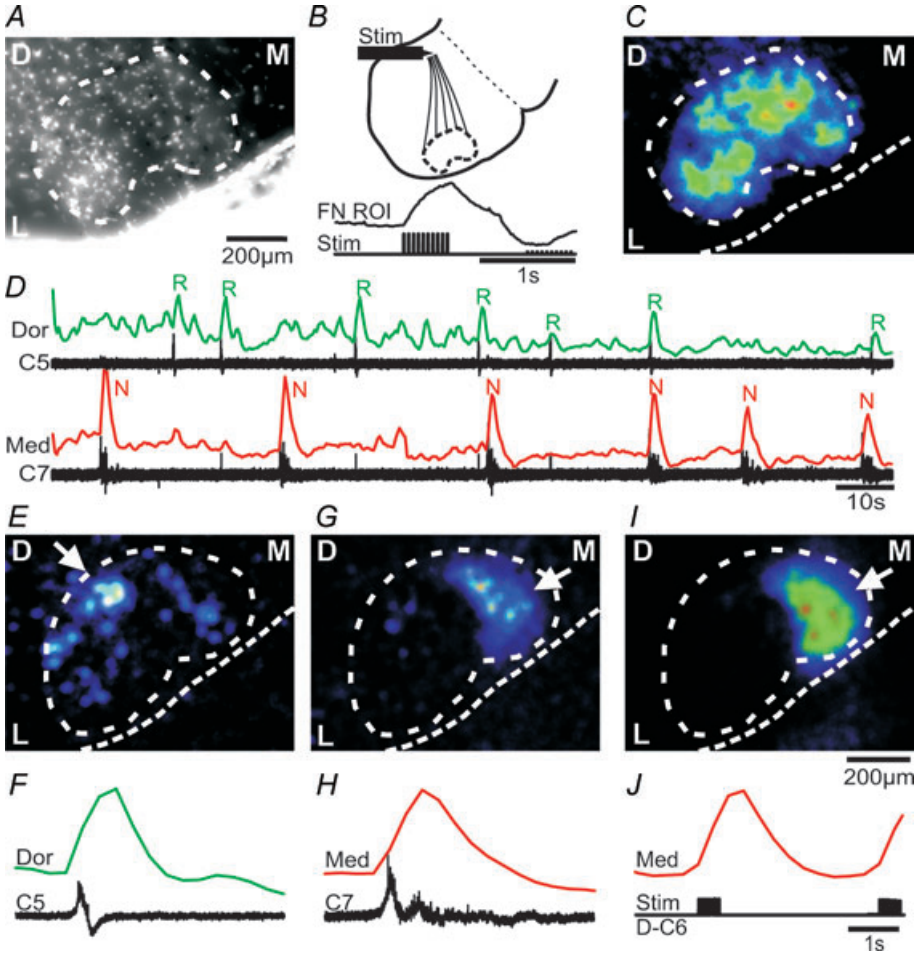

Figure 4. Respiratory activity in dorsal, lateral and medial facial subnuclei, and novel motor activity in the medial facial subnucleus
A, average Z-stack-projection of a raw Fluo-8 AM image stack (900 images) from a mid-facial brainstem–spinal cord preparation. D, dorsal; M, medial; L, lateral. Note that the density of facial motoneurons creates an approximate outline (white dotted line) of the facial nucleus. *B*, diagram illustrating the position (at the internal facial genu) of a stimulating electrode (Stim) used to antidromically activate facial motoneurons. Lower trace, stimulus timing and the resulting ΔF over the facial nucleus (FN ROI). *C*, CTA image from the facial nucleus triggered off antidromic stimuli (9 stimuli) of the internal facial genu. Calibration bar in *A* applies to *C*. *D*, spontaneous respiratory (R) and novel motor (N) nerve activity recorded from cervical (C5, C7) rootlets, and traces showing the ΔF over the dorsal (Dor, green trace) and medial (Med, red trace) facial subnuclei. *E*, CTA image from the facial nucleus triggered off respiratory activity on C5 (6 cycles). Note the strong ΔF signal from the dorsal (arrow) and weaker signal from the lateral and medial subnuclei. *F*, averages of respiratory nerve activity (C5) and ΔF trace from the dorsal (Dor) facial subnucleus. *G*, CTA image from the facial nucleus triggered off novel motor nerve activity on C7 (6 cycles). *H*, averages of novel motor nerve activity (C7) and ΔF trace from the medial (Med) facial subnucleus. *I*, CTA image from the facial nucleus triggered off dorsal root stimulation of the D–C6 (11 stimuli). *J*, dorsal root stimulus timing, and ΔF trace from the medial (Med) facial subnucleus. Note the strong ΔF signal from the medial subnucleus in *G* and *I* (arrow).

(2.9 ± 0.8 burst min^{-1}) in the medial subnucleus, without concomitant novel motor activity on cervical nerves, was recorded in six separate experiments, and this activity was not synchronized with respiratory nerve activity (not shown). Cervical dorsal root stimulation, using the same protocol as in the brainstem–spinal cord preparations, induced activity in the medial facial subnucleus, overlapping with the activity seen during spontaneous novel motor activity (Fig. 4*I* and *J*, supplementary movie 2). Group data showed that stimulation of dorsal root C2, C4–8 and T3 triggered strong activity in medial facial subnucleus ($n = 11$ mid-facial brainstem–spinal cord preparations). Stimulation of cervical ventral roots at the same spinal levels gave no response.

Facial subnuclei and cellular timing at high temporal resolution

Image acquisition at 3 frames s^{-1} (Figs 1–4 experiments) was too slow to reveal a possible time sequence of subregional activities in relation to nerve burst activities. Imaging at 70 frames s^{-1} was therefore performed in parallel with nerve recordings, at the cost of spatial resolution (camera EMCCD 2×2 binning). Several sequential image stacks were combined to create recordings with multiple respiratory burst events, focusing the analysis on facial dorsal, lateral and medial subnuclei (Fig. 5*A* and *B*). CTA images of facial nucleus activity before, during and after the respiratory nerve peak were obtained to possibly identify regional distributions of activity along the event of the burst (Fig. 5*C* and *D*). No dominant regional activity within the facial nucleus was seen before the nerve burst (Fig. 5*C*, Before). Strong dorsal and lateral facial activity was seen during the early phases of the respiratory nerve burst (Fig. 5*C*, During). Interestingly, medial facial activity was seen later during the respiratory nerve burst (Fig. 5*C*, After). Averages of respiratory activity on the cervical nerve and ΔF from the facial subnuclei showed that calcium activity started first in the dorsal subnucleus (at -230 ± 160 ms before nerve onset), tightly followed by initiation in the lateral subnucleus (at -200 ± 160 ms), and thereafter initiation of the medial subnucleus (-50 ± 50 ms, $n = 9$ cycles). Peak of the calcium signal relative to peak of the nerve burst activity was 320 ± 60 ms for the dorsal, 370 ± 100 ms for the lateral, and 550 ± 27 ms for the medial subnucleus. Group data from mid-facial brainstem–spinal cord preparations imaged at 70 frames s^{-1} gave dorsal initiation at -90 ± 83 ms ($P < 0.05$ compared to lateral initiation, paired t test), lateral initiation at -79 ± 57 ms, and medial initiation at 14 ± 57 ms ($n = 3$). Individual cells within the dorsal subnucleus could optically be resolved in a few experiments at 70 frames s^{-1} ($n = 2$), and some cells showed activity synchronized with some, but not all, respiratory nerve bursts (Fig. 5*E*, cells *a–d*), while others were synchronized with all bursts (Fig. 5*E*, cells *e–h*). Cells active only at some respiratory bursts initiated activity 160 ± 60 ms before the nerve burst, whereas cells active at all respiratory bursts initiated activity in closer proximity to the start of the nerve burst (90 ± 50 ms, $P < 0.05$). In the two experiments with clear cellular resolution, individual facial motoneurons displayed a sequential pattern of activation (Fig. 5*G–J*). During a single respiratory nerve burst the activity in Early cells (starting 211 ± 18 ms before the nerve onset, $n = 4$ cells), appeared in the dorsal facial subnucleus, followed by activity in Initial cells (27 ± 17 ms before the nerve onset, $n = 11$ cells, $P < 0.001$) and Late cells (247 ± 67 ms after the nerve onset, $n = 11$ cells, $P < 0.001$), located more lateral and medial within the facial nucleus. Thus, respiratory calcium activity within the facial nucleus started dorsally, and then appeared more lateral and medial (Fig. 5*J*).

The rostrocaudal extension of the respiratory calcium signal within the facial nucleus was investigated in brainstem–spinal cord preparations with one side trimmed by the vibrating-blade microtome in the sagittal plane to expose the respiratory column and the facial nucleus (Fig. 6, $n = 4$). Respiratory calcium activity was noted throughout the dorsal part of the facial nucleus, in particular from the midpoint to the caudal border, and peak amplitudes were larger in the dorsal than in the ventral part of the facial nucleus ($213 \pm 38\%$, $P < 0.01$, $n = 4$, Fig. 6*A* and *B*). The respiratory calcium signal in the facial nucleus was synchronized with a much stronger signal in the respiratory column located immediately caudal to the nucleus (Fig. 6*A* and *B*). Calcium imaging was followed by whole mount immunolabelling using antibodies against ChAT, confirming the location of the facial nucleus ($n = 3$), which could be distinguished clearly from the more caudal respiratory column (not shown).

Electrical field potential and whole-cell patch recordings from the facial nucleus

A variant of the mid-facial brainstem–spinal cord preparation where one half of the upper brainstem was retained and a cut was placed through the mid-facial nucleus in the other half was used to record electrical field potentials from the facial nucleus (Fig. 7*A*). A field potential recording pipette was placed systematically at eight positions (*a–h*) within the facial nucleus (Fig. 7*B*), and VII nerve activity was recorded from the contralateral side. The boundary of the facial nucleus was visible in the stereomicroscope as a transition of large soma cells to smaller cells (Fig. 7*B*, dotted line). This type of preparation showed large-amplitude respiratory burst activity on the VII nerve with a frequency of

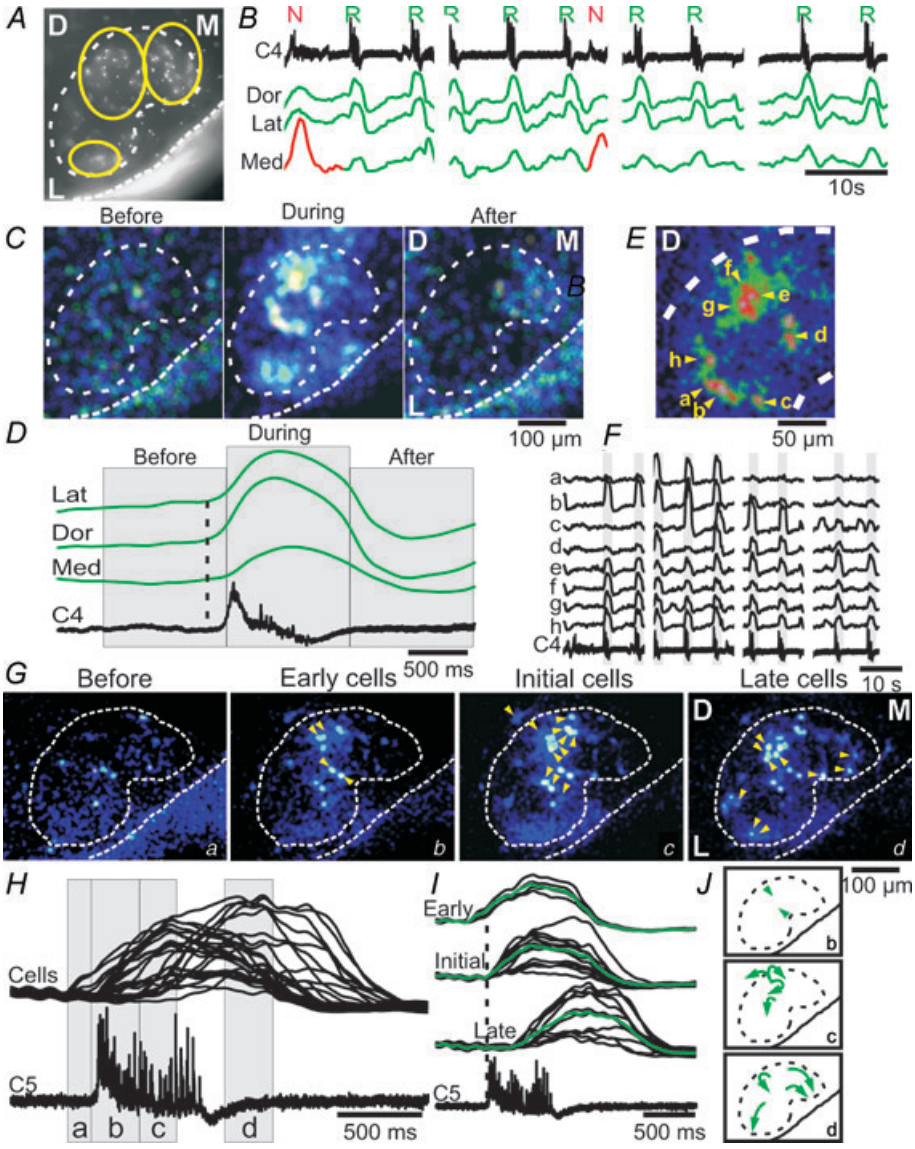

Figure 5. Respiratory activity starts in the dorsal facial subnucleus
A, average Z-stack-projection of a raw Fluo-8 AM image stack (4 × 450 images, 2 × 2 binning) from a mid-facial brainstem–spinal cord preparation. D, dorsal; M, medial; L, lateral. Yellow circles define the dorsal, lateral and medial ROIs used for analysis in *B–D*. *B*, spontaneous nerve activity recorded from cervical (C4) rootlet, and traces showing the ΔF over the dorsal (Dors), lateral (Lat) and medial (Med) facial subnuclei based on four 70 frames s^{-1} image sessions. Note the respiratory activity in the dorsal, lateral and medial subnuclei (green traces), and the novel motor activity in the medial subnucleus (red trace). *C*, CTA images from the facial nucleus triggered off respiratory activity on C4 (9 cycles) in time frames termed 'Before' (corresponding to the time in indicated in *D*), 'During' and 'After' the respiratory nerve activity. *D*, averages of respiratory activity (C4) and ΔF traces from the lateral (Lat), dorsal (Dors) and medial (Med) facial subnuclei. Note that the medial subnucleus starts and peaks later than the dorsal and lateral subnuclei (dotted line). *E*, high magnification CTA image from the dorsal facial nucleus triggered off cervical nerve (C4, 9 cycles) showing the somatic location of eight (*a–h*) putative facial motoneurons. *F*, traces showing ΔF from each of the eight neurons in *E*, along with the C4 respiratory activity. Note that neurons *a–d* show activity synchronized with some, but not all, respiratory nerve bursts, whereas neurons *e–h* are synchronized with all respiratory bursts. *G*, low magnification CTA images from the facial nucleus, with cellular resolution (yellow triangles), in timeframes termed 'Before' (corresponding to the time (*a*) indicated in *H*), 'Early cells' (time *b* in *H*), 'Initial cells' (time *c* in *H*) and 'Late cells' (time d in *H*). *H*, overlaid ΔF traces from cells shown in *G*, in relation to a single respiratory burst on C5. *I*, sorted traces showing ΔF from Early, Initial and Late cells, and the resulting average (green traces), in relation to a single respiratory burst on C5. *J*, schematic diagram showing the dorsal start of respiratory activity, and subsequent spread to lateral and medial facial subnuclei.

5.8 ± 2.1 bursts min^{-1} ($n = 6$), and small-amplitude faster burst activity of 41.5 ± 2.5 bursts min^{-1} ($n = 2$ of 6). The faster amplitude burst activity ran down after 20 min in both preparations, leaving behind the large-amplitude burst activity (not shown). Recordings showed field potentials in synchrony with the large-amplitude bursts on the contralateral facial nerve in positions that were predominantly dorsal (positions *b* and *c*, in 50–100% of the experiments), and lateral (positions *a*, *e* and *f*, in 30–60% of the experiments, $n = 6$, Fig. 7*B*). No synchronized field potential activity was noted in the more medial positions (position *d*, *g* and *h*, $n = 6$), or in synchrony with the small-amplitude burst activity ($n = 2$). Whole-cell recordings from facial motoneurons (resting V_m: −69 ± 1 mV, Input resistance: 295 ± 201 MΩ) in the dorsal and lateral area of the facial nucleus showed weak respiratory drives (5.7 ± 2.9 mV) without spike activity synchronized with respiratory activity on cervical nerves (Fig. 7*D*–*G*, $n = 4$).

Respiratory-modulated facial premotoneurons located dorsomedial to the facial nucleus

Calcium imaging of cells located outside the facial nucleus revealed respiratory activity in putative facial premotoneurons (Fig. 8). A CTA image triggered off the respiratory C4 nerve bursts ($n = 18$) showed strong respiratory activity in the dorsal and lateral facial subnuclei, but also in a region located dorsomedial to the facial nucleus (Fig. 8*A*, supplementary movie 3). A zoom-in of the dorsomedial region (Fig. 8*A*, yellow square) showed individual putative premotoneurons ($n = 12$, Fig. 8*B*, yellow arrows) with respiratory activity. ROIs encircling each of the individual cells revealed ΔF traces that clearly showed synchronized activity with respiratory activity on C4, and the dorsal and medial facial subnuclei (Fig. 8*C* and *D*). A cumulated diagram overlaying the position of respiratory-modulated facial premotoneurons from eight preparations (60 cells in total) showed a predominant location dorsal and dorsomedial to the facial nucleus (Fig. 8*E*).

Discussion

Electrical field potential recordings and population calcium imaging of the ventral brainstem surface and the facial nucleus revealed strong respiratory activity in dorsal and lateral facial subnuclei, indicating that patterned activation of facial muscles during breathing is functional in very young animals. The current study also uncovered a novel motor activity on facial and cervical nerves, possibly generated by neurons located in an elongated column in the ventromedial brainstem.

The facial nucleus in adult mice is organized somatotopically with seven identifiable subnuclei that innervate facial and auricular muscles (Ashwell, 1982; Komiyama *et al.* 1984; Terashima *et al.* 1993). Notably, the nasolabial muscles receive innervation from the lateral and dorsolateral subnucleus, the platysma and mentalis muscles from the dorsal and ventral intermediate subnucleus, the posterior belly of the digastric muscle from the accessory facial subnucleus, and the auricular muscles from the dorso- and ventromedial subnuclei. In the current study particularly strong respiratory activity was noted in the dorsal and lateral facial subnuclei, which according to the musculotopic organization contain motoneurons innervating the nasolabial, platysma, mentalis and possibly digastric muscles. Indeed *in vivo* experiments, albeit in other species, have demonstrated

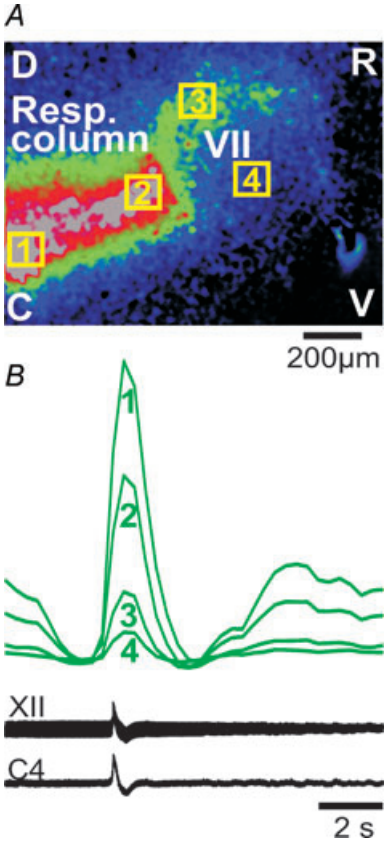

Figure 6. Respiratory activity is strongest in the dorsal part of the facial nucleus in the sagittal plane
A, CTA image from the respiratory column and facial nucleus captured in the sagittal plane triggered off respiratory activity on C4 (19 cycles). D, dorsal; V, ventral; C, caudal; R, rostral. Yellow squares define four ROIs used for the analysis in *B*. Note the strong ΔF signal from the dorsal (ROI-3) and weaker signal from the ventral part of the facial nucleus (ROI-4). *B*, averages of respiratory nerve activity (XII, C4, black traces) and ΔF (green traces) from the caudal and rostral respiratory column (lines 1 and 2), and dorsal and ventral part of the facial nucleus (lines 3 and 4). Note that the peak dorsal ΔF signal (line 3) is larger than the peak ventral ΔF signal.

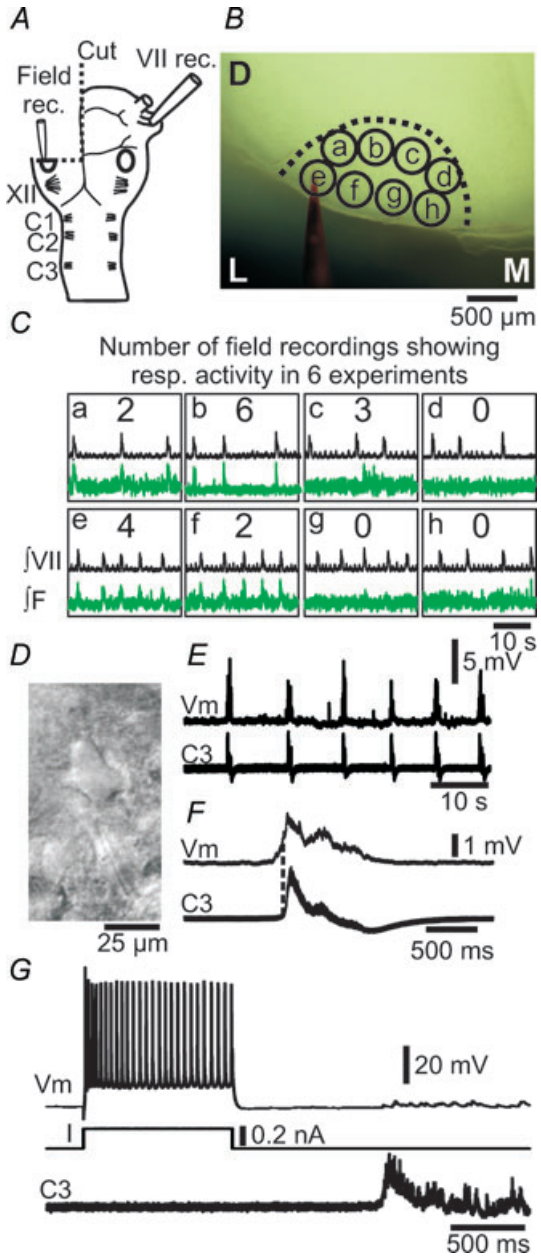

Figure 7. Electrical field potential recordings from the facial nucleus show respiratory activity in dorsal and lateral subnuclei
A, brainstem–spinal cord preparation, with one-side transverse cut through the mid-facial nucleus (oval), illustrating the position of nerve and field potential recording pipettes. VII, facial nerve; XII, hypoglossal rootlets; C1, first cervical nerve. *B*, photomicrograph of the live preparation, indicating the outline of the facial nucleus, eight recording positions (*a*–*h*), and the field potential recording pipette (labelled with red dye). D, dorsal; L, lateral; M, medial. *C*, integrated facial nerve, and field potential recordings (green traces) from positions *a*–*h* within the facial nucleus (∫VII, ∫F). Numbers in the middle of each box indicate the number of field potential recordings showing respiratory activity in 6 experiments. Note that the dorsal and lateral positions show respiratory field potential activity. *D*, contrast enhanced video micrograph of facial motoneuron. *E*, whole-cell patch recording of weak inspiratory drive potentials in a facial motoneuron (V_m), along with respiratory nerve activity on C3. *F*, cycle triggered average (6 cycles) of the membrane potential (V_m) and C3 activity from *E*. Dotted line indicates onset of nerve activity. *G*, firing pattern of a facial motoneuron in response to current (*I*) input, a single respiratory nerve burst on C3 and the resulting small inspiratory burst potential.

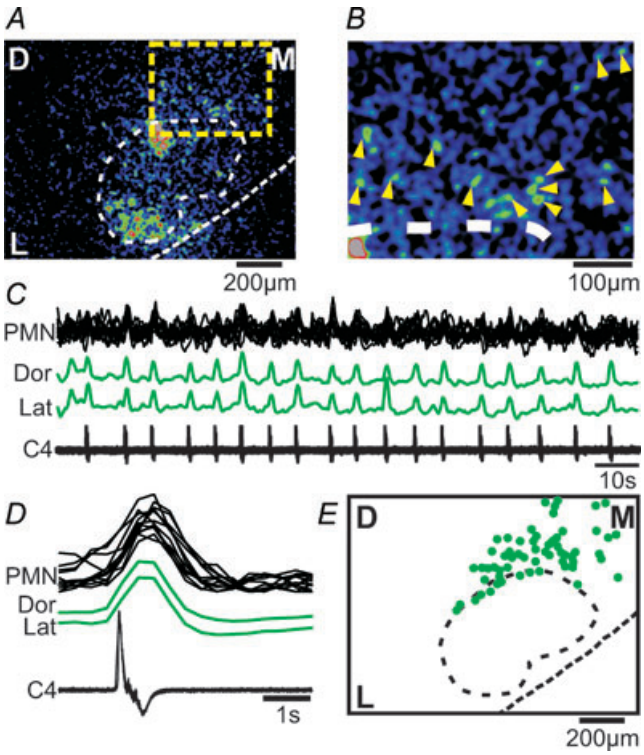

Figure 8. Putative facial premotoneurons, located dorsomedial to the facial nucleus, show respiratory activity
A, CTA image from the facial nucleus triggered off respiratory activity on C4 (18 cycles) showing respiratory activity in the dorsal and lateral facial subnuclei, but also in cells located outside the facial nucleus (yellow square). *B*, zoom in of the yellow square region from *A*, showing individual cells (yellow triangles). *C*, respiratory activity on C4 and Δ*F* traces from the dorsal (Dor) and lateral (Lat) facial nucleus, and from individual premotoneurons (PMN, black overlaid traces). *D*, averages of respiratory activity (C4) and Δ*F* traces from 12 PMNs located dorsomedially to the facial nucleus. *E*, cumulated location of facial premotoneurons (green filled circles) showing respiratory activity (from 8 preparations). Note the predominantly dorsomedial positions of respiratory-modulated facial premotoneurons.

respiratory modulated activity in the nasolabial muscles (man, dogs, rat, cat, rabbit; Mann *et al.* 1977; Sherrey & Megirian, 1977; Bystrzycka & Nail, 1983; Mathew, 1984; Terndrup *et al.* 1996). Activation of ala nasi muscles results in a decrease in nasal and total respiratory resistance (Mathew, 1984). The platysma and digastric muscles show respiratory-modulated activity under high respiratory drive (De *et al.* 1986; Saiki & Matsumoto, 2004), the

mentalis muscle under quiet breathing (Dutra *et al.* 2006). Thus, we surmise that the brainstem of newborn mice already has in place the pattern forming circuits that are necessary to activate the parts of the facial nucleus needed to maintain airway patency. The dorsal subnucleus was the first to be activated during an inspiratory burst, which may indicate that a specific temporal sequence of activation of facial subnuclei is produced at this early age, with the muscles around the mouth being activated before the ala nasi. Since we only recorded calcium signals at the level of the mid-facial nucleus, we cannot exclude that more rostral or caudally located subnuclei may also be strongly respiratory modulated. We assume that the calcium signal in the facial nucleus comes from facial motoneurons, also because we recorded from a small sample of neurons using whole-cell patch clamp, and these cells had typical motoneuron properties. However, the facial nucleus in adult rats also contains respiratory-modulated neurons that are not motoneurons (Li *et al.* 2004; Zhang *et al.* 2004), and the optical data presented here could consequently also represent activity in these intriguing neurons, which have yet to be studied in detail. Some facial motoneurons were active only at some respiratory bursts, others were active at all respiratory bursts, and the latter group initiated activity in closer proximity to the start of the nerve burst. This variation may result from dendrites being cut during the dissection, reducing afferent input in some neurons. However, presumed pFRG neurons at the brainstem surface showed similar properties, suggesting that cycle-to-cycle variations in synaptic drive to respiratory neurons may result in cells being in and out of the network at different times.

Neurons located dorsomedial to and outside of the facial nucleus in the current study showed respiratory-modulated activity. We propose that these neurons might be facial premotoneurons since retrograde studies in rat show reticular facial premotoneurons at this anatomical location (Travers & Norgren, 1983; Dauvergne *et al.* 2001; Hattox *et al.* 2002). Some of these neurons were located just at the border of the facial nucleus, and thus may in fact be proper facial motoneurons. Anatomical and functional studies show that the facial nucleus receives synaptic input from many areas in the medulla, including regions that contain respiratory neurons such as the rostral ventral respiratory group, the nucleus tractus solitarii, the parabrachial nucleus, the Kölliker–Fuse region and the pFRG (Bystrzycka & Nail, 1983; Ellenberger & Feldman, 1990; Lin & Hwang, 1994; Zheng *et al.* 1998; Hattox *et al.* 2002; Onimaru *et al.* 2006). Thus, the facial nucleus may receive respiratory-related inputs directly from several sources, but the current study also suggests that part of this drive may pass through closely located premotoneurons.

The exact cellular identity of the population of respiratory-modulated neurons at the surface of the ventrolateral brainstem remains to be determined. The region clearly corresponds to the location of the pFRG previously identified using optical and electrical recordings (Onimaru & Homma, 2003; Onimaru *et al.* 2006), and thus may contain the proposed secondary brainstem respiratory oscillator (Dubreuil *et al.* 2009; Onimaru *et al.* 2009; Thoby-Brisson *et al.* 2009). However, we speculate that some of the calcium signal may stem from the underlying facial nucleus. Penetration of the calcium sensitive dye is probably in the order of $\sim$60 μm (Funke *et al.* 2007), and therefore the dye could reach facial motoneurons located close to the surface. Pre-I neurons located in the pFRG often show fast oscillatory bursts in between inspiratory activity (Onimaru *et al.* 2006), activity that can be seen on recordings from facial nerves indicating that this population of cells also drives the facial motor pool. Fast oscillatory activity on the facial nerve in the current study was also seen in a few experiments, but ran down within 20 min. The fast oscillatory burst observed here had a higher frequency than those reported by Onimaru *et al.* 2006 (42 bursts min^{-1} *versus* 7 bursts min^{-1}), suggesting that the preparations used here may be in a state of increased excitability, which could overwhelm the fast oscillatory processes in the pFRG. Thus, we speculate that both of the preparations used here are in a state where the pre-I neurons do not produce fast oscillations, and that the activity of the pFRG may be in a one-to-one entrainment with the activity of the preBötzinger complex.

A novel motor activity on facial, cervical and thoracic nerves was observed in the current study. The nerve discharges were synchronized with calcium signals at the surface of the ventromedial brainstem, and cervical dorsal root stimulation induced similar ventromedial activity. The frequency and occurrence of the novel motor activity was lower in the mid-facial brainstem–spinal cord preparations (2.9 burst min^{-1} in 10% of the preparations) than in the brainstem–spinal cord preparation (10.2 burst min^{-1} in 30% of the preparations). We suspect that removal of the pia mater in the brainstem–spinal cord preparation, which was not done in the mid-facial brainstem–spinal cord preparation, may affect the integrity or excitability of neurons located close to the surface, which in turn could affect the occurrence or frequency of the novel motor activity. The transverse cut that ran through the ventromedial brainstem which showed calcium activity synchronized with the novel motor activity on the cervical nerves, could also lesion part of the neuronal population involved in the generation of the novel motor activity. Experiments, using the mid-facial brainstem–spinal cord preparation demonstrated that the medial facial subnucleus has calcium signals synchronized with this novel motor activity on cervical nerves, and cervical dorsal root stimulation induced similar medial facial subnucleus

activity. The function associated with this novel activity remains unknown. It could be an artifact of the *in vitro* condition. However, we postulate that the activity reflects some form of motor behaviour involving at least facial, upper body and possibly forelimb muscles since the novel motor output was recorded on the facial nerve and C1–T3 ventral spinal roots. Co-activity could be recorded on ipsilateral nerves and the associated optical calcium signal at the brainstem surface showed left–right synchronization. We therefore suggest that the behaviour may involve co-contraction of a large number of muscles on both sides of the animal. The distinct activation of the medial facial subnucleus, which innervates auricular muscles, suggests that the motor behaviour involve either ear orientation or mouth opening, resulting from activation of muscles connecting the ear and mouth region, such as during a squeak. The spontaneous and dorsal root stimulation-induced ventromedial activity, recorded at the brainstem surface, formed a bilateral elongated column extending caudally from the level of the medial facial nucleus, with particularly strong signals at the rostral and caudal pole. The anatomical identity of neurons in this column remains to be determined, but they clearly include the medial facial nucleus, and may include the paragigantocellular reticular nucleus and the lateral reticular nucleus. Neurons with somas located at the brainstem surface showed ventromedial calcium signals. Thus, it is also possible that the column in fact is very superficial and mainly contains neurons located in the narrow space between the above mentioned regions and the surface. However, it is noteworthy that the paragigantocellular reticular nucleus has descending spinal projections terminating in the ventral horn at all levels of the spinal cord, and has been proposed to be involved in multiple behaviours with somatic and autonomic components, such as reproductive reflexes, acoustic startle and nociception (Hermann *et al.* 2003). We consider a nociceptive reflex, involving defensive motor contraction of the entire upper body and facial activity involved in producing a squeak, a possible candidate for the novel motor activity reported here. The fact that the ventromedial activity could be elicited by dorsal root stimulation supports the notion that the behaviour is induced by somatosensory input. We do not consider it likely that the novel activity represents gasping. Gasping-related optical signals at the brainstem surface overlap (slightly caudally and dorsally shifted) with inspiratory regions during eupnoea in juvenile rats, a region which does not correspond to the ventromedial region identified here (Potts & Paton, 2006). However, we cannot exclude the possibility that the activity involves activation of the respiratory musculature, but experiments on less reduced preparations are warranted to determine this. The novel motor activity could also represent coordinated motor signals important for development of circuits and networks. However, the spontaneous embryonic activity, which is recorded on facial nerves (Gust *et al.* 2003), disappears from the hindbrain at E14.5, well before the age of the animals used here (Bosma, 2010). Controlled lesion and other activity promoting or blocking experiments are needed to identify the source of the novel activity. The question arises of why this novel motor activity has not been reported before, since many studies have used similar preparations, albeit in newborn rats. We suspect that the composition of the ACSF, with a substantially lower extracellular calcium concentration (0.8 mM) than normally used, may have uncovered the novel activity. Low extracellular calcium was used to increase excitability of the preparations used here (Rekling *et al.* 1996; Panaitescu *et al.* 2010), which otherwise would not produce spontaneous respiratory activity (Jean-Charles & Gerard, 2002).

In conclusion, specific facial subnuclei receive strong respiratory drive, which may be necessary to maintain airway patency by controlling the order and strength of facial muscle contractions. In addition, a novel pattern forming circuit is present in the ventromedial brainstem, which may drive the medial facial subnucleus and cervical motor pools.

References

Ashwell KW (1982). The adult mouse facial nerve nucleus: morphology and musculotopic organization. *J Anat* **135**, 531–538.

Bosma MM (2010). Timing and mechanism of a window of spontaneous activity in embryonic mouse hindbrain development. *Ann N Y Acad Sci* **1198**, 182–191.

Bouvier J, Thoby-Brisson M, Renier N, Dubreuil V, Ericson J, Champagnat J, Pierani A, Chedotal A & Fortin G (2010). Hindbrain interneurons and axon guidance signalling critical for breathing. *Nat Neurosci* **13**, 1066–1074.

Bystrzycka EK & Nail BS (1983). The source of the respiratory drive to nasolabialis motoneurones in the rabbit; a HRP study. *Brain Res* **266**, 183–191.

Dauvergne C, Pinganaud G, Buisseret P, Buisseret-Delmas C & Zerari-Mailly F (2001). Reticular premotor neurons projecting to both facial and hypoglossal nuclei receive trigeminal afferents in rats. *Neurosci Lett* **311**, 109–112.

De Troyer A, Estenne M & Vincken W (1986). Rib cage motion and muscle use in high tetraplegics. *Am Rev Respir Dis* **133**, 1115–1119.

Drummond GB (2009). Reporting ethical matters in *The Journal of Physiology*: standards and advice. *J Physiol* **587**, 713–719.

Dubreuil V, Thoby-Brisson M, Rallu M, Persson K, Pattyn A, Birchmeier C, Brunet JF, Fortin G & Goridis C (2009). Defective respiratory rhythmogenesis and loss of central chemosensitivity in Phox2b mutants targeting retrotrapezoid nucleus neurons. *J Neurosci* **29**, 14836–14846.

Dutra EH, Maruo H & Vianna-Lara MS (2006). Electromyographic activity evaluation and comparison of the orbicularis oris (lower fascicle) and mentalis muscles in predominantly nose- or mouth-breathing subjects. *Am J Orthod Dentofacial Orthop* **129**, 722–729.

Ellenberger HH & Feldman JL (1990). Brainstem connections of the rostral ventral respiratory group of the rat. *Brain Res* **513**, 35–42.

Fay RA & Norgren R (1997). Identification of rat brainstem multisynaptic connections to the oral motor nuclei in the rat using pseudorabies virus. II. Facial muscle motor systems. *Brain Res Brain Res Rev* **25**, 276–290.

Feldman JL & Del Negro CA (2006). Looking for inspiration: new perspectives on respiratory rhythm. *Nat Rev Neurosci* **7**, 232–242.

Funke F, Dutschmann M & Muller M (2007). Imaging of respiratory-related population activity with single-cell resolution. *Am J Physiol Cell Physiol* **292**, C508–C516.

Gust J, Wright JJ, Pratt EB & Bosma MM (2003). Development of synchronized activity of cranial motor neurons in the segmented embryonic mouse hindbrain. *J Physiol* **550**, 123–133.

Hattox AM, Priest CA & Keller A (2002). Functional circuitry involved in the regulation of whisker movements. *J Comp Neurol* **442**, 266–276.

Hermann GE, Holmes GM, Rogers RC, Beattie MS & Bresnahan JC (2003). Descending spinal projections from the rostral gigantocellular reticular nuclei complex. *J Comp Neurol* **455**, 210–221.

Jean-Charles V & Gerard H (2002). Noradrenergic receptors and in vitro respiratory rhythm: possible interspecies differences between mouse and rat neonates. *Neurosci Lett* **324**, 149–153.

Komiyama M, Shibata H & Suzuki T (1984). Somatotopic representation of facial muscles within the facial nucleus of the mouse. A study using the retrograde horseradish peroxidase and cell degeneration techniques. *Brain Behav Evol* **24**, 144–151.

Lang IM (2009). Brain stem control of the phases of swallowing. *Dysphagia* **24**, 333–348.

Li C, Guan Z, Chan Y & Zheng Y (2004). Projections from facial nucleus interneurons to the respiratory groups of brainstem in the rat. *Neurosci Lett* **368**, 25–28.

Lin CY & Hwang JC (1994). Responses of respiratory-modulated facial nerve activity to activation of the ventrolateral subarea of the nucleus of the tractus solitarius. *Chin J Physiol* **37**, 185–191.

Mann DG, Sasaki CT, Fukuda H, Mann DG, Suzuki M & Hernandez JR (1977). Dilator naris muscle. *Ann Otol Rhinol Laryngol* **86**, 362–370.

Manzini I, Schweer TS & Schild D (2008). Improved fluorescent (calcium indicator) dye uptake in brain slices by blocking multidrug resistance transporters. *J Neurosci Methods* **167**, 140–147.

Mathew OP (1984). Upper airway negative-pressure effects on respiratory activity of upper airway muscles. *J Appl Physiol* **56**, 500–505.

Onimaru H & Homma I (2003). A novel functional neuron group for respiratory rhythm generation in the ventral medulla. *J Neurosci* **23**, 1478–1486.

Onimaru H, Ikeda K & Kawakami K (2009). Phox2b, RTN/pFRG neurons and respiratory rhythmogenesis. *Respir Physiol Neurobiol* **168**, 13–18.

Onimaru H, Kumagawa Y & Homma I (2006). Respiration-related rhythmic activity in the rostral medulla of newborn rats. *J Neurophysiol* **96**, 55–61.

Panaitescu B, Ruangkittisakul A & Ballanyi K (2010). Depression by Ca^{2+} and stimulation by K^{+} of fictive inspiratory rhythm in newborn rat brainstem slices. *Adv Exp Med Biol* **669**, 91–95.

Potts JT & Paton JF (2006). Optical imaging of medullary ventral respiratory network during eupnea and gasping in situ. *Eur J Neurosci* **23**, 3025–3033.

Rekling JC, Champagnat J & Denavit-Saubie M (1996). Electroresponsive properties and membrane potential trajectories of three types of inspiratory neurons in the newborn mouse brain stem in vitro. *J Neurophysiol* **75**, 795–810.

Rybak IA, Abdala AP, Markin SN, Paton JF & Smith JC (2007). Spatial organization and state-dependent mechanisms for respiratory rhythm and pattern generation. *Prog Brain Res* **165**, 201–220.

Saiki C & Matsumoto S (2004). Digastric muscle activities in anoxic infant rats. *Can J Physiol Pharmacol* **82**, 960–968.

Sherrey JH & Megirian D (1977). State dependence of upper airway respiratory motoneurons: functions of the cricothyroid and nasolabial muscles of the unanesthetized rat. *Electroencephalogr Clin Neurophysiol* **43**, 218–228.

Strohl KP (1985). Respiratory activation of the facial nerve and alar muscles in anaesthetized dogs. *J Physiol* **363**, 351–362.

Terashima T, Kishimoto Y & Ochiishi T (1993). Musculotopic organization of the facial nucleus of the reeler mutant mouse. *Brain Res* **617**, 1–9.

Terndrup TE, Knuth SL, Gdovin MJ, Darnall R & Bartlett D Jr (1996). Respiratory motor nerve activities during experimental seizures in cats. *J Appl Physiol* **80**, 924–930.

Thoby-Brisson M, Karlen M, Wu N, Charnay P, Champagnat J & Fortin G (2009). Genetic identification of an embryonic parafacial oscillator coupling to the preBotzinger complex. *Nat Neurosci* **12**, 1028–1035.

Travers JB & Norgren R (1983). Afferent projections to the oral motor nuclei in the rat. *J Comp Neurol* **220**, 280–298.

Ye JH, Zhang J, Xiao C & Kong JQ (2006). Patch-clamp studies in the CNS illustrate a simple new method for obtaining viable neurons in rat brain slices: glycerol replacement of NaCl protects CNS neurons. *J Neurosci Methods* **158**, 251–259.

Zhang C, Yan H, Li C & Zheng Y (2004). Possible involvement of the facial nucleus in regulation of respiration in rats. *Neurosci Lett* **367**, 283–288.

Zheng Y, Riche D, Rekling JC, Foutz AS & Denavit-Saubie M (1998). Brainstem neurons projecting to the rostral ventral respiratory group (VRG) in the medulla oblongata of the rat revealed by co-application of NMDA and biocytin. *Brain Res* **782**, 113–125.

Author contributions

K.P. and J.C.R. contributed to the conception and design of the experiments and contributed to the collection, analysis and interpretation of data. All authors contributed to drafting the article or revising it critically for important intellectual content. All authors approved the final version of the manuscript.

Acknowledgements

This work was supported by Danish Medical Council, the NovoNordisk Foundation, Den Owensenke Fond, Lægeforeningens forskningsfond, and Agnes og Pouls Friis Fond. We thank Lis Hansen for technical assistance.